Wiley
International Journal of RF and Microwave Computer-Aided Engineering
Volume 2025, Article ID 2346639, 12 pages
https://doi.org/10.1155/mmce/2346639

WILEY

Research Article

Selective Manipulation of Microwaves by a Cascade of Independent Metasurfaces Based on Planar Spirals

Ivan Fanyaev,[1] **Andrei Samofalov**,[2] **Alexander Kravchenko**,[3] **Dazhi Ding**,[4] **Mengmeng Li**,[4] **Igor Semchenko**,[5] **Sergei Khakhomov**,[6] **and Ihar Faniayeu**[7]

[1]*Department of Radiophysics and Electronics, Francisk Skorina Gomel State University, Gomel, Belarus*
[2]*Department of General Physics, Francisk Skorina Gomel State University, Gomel, Belarus*
[3]*Belarusian Scientific Research and Design Institute of Oil, Belorusneft, Gomel, Belarus*
[4]*School of Microelectronics and the School of Integrated Circuits, Nanjing University of Science and Technology, Nanjing, China*
[5]*State Scientific and Production Association "Optics, Optoelectronics and Laser Technology", National Academy of Sciences of Belarus, Minsk, Belarus*
[6]*Department of Optics, Francisk Skorina Gomel State University, Gomel, Belarus*
[7]*Department of Physics, University of Gothenburg, Gothenburg, Sweden*

Correspondence should be addressed to Ihar Faniayeu; ihar.faniayeu@physics.gu.se

Received 5 December 2024; Revised 2 June 2025; Accepted 27 June 2025

Academic Editor: Mohammad Rezwan Habib

We propose a multifunctional cascade metasurface designed for manipulating electromagnetic waves in the microwave frequency range with comprehensive theoretical analysis, design optimization, and experimental validation. A set of electrically thin metasurfaces based on planar spirals with free space impedance is used to manipulate electromagnetic waves. The metasurfaces simultaneously generate distinct, independent, and mutually compatible wave transformations at various frequencies. A multifunctional cascade metasurface integrates several functional devices, including a reflective cross-polarizer, a transmissive cross-polarizer, and a nonreflective absorber. Each designed metasurface has a free space impedance over a sufficiently wide frequency range that encompasses the operating frequencies of all metasurfaces. This attribute guarantees the autonomous and mutually noninterfering functioning of all metasurfaces in the cascade.

Keywords: absorber; cross-polarizer; free space impedance; metasurface; microwave range

1. Introduction

As a relatively young field of science, the electrodynamics of metamaterials (MMs) has created immense possibilities for controlling electromagnetic waves across a significant frequency spectrum, ranging from microwaves to visible radiation. The resulting MMs have the ability to perform various functions, including object cloaking, visualization, ideal absorption, negative refraction [1–5], anomalous refraction and reflection [6], effective scattering area reduction [7], focusing [8], electromagnetic wave diffusion [9, 10], vortex beam generation [11–14], and holography [15]. Irrespective of the underlying mechanism of each application, all of their many features are achieved by manipulating the fundamental properties of electromagnetic phenomena during their propagation [16, 17]. MMs typically consist of continuous macroscopic media with effective "ε" and "μ." Their properties can be explained using the effective medium theory [18–20]. Despite the advancements in electromagnetic field control achieved through the use of MMs, the manufacture of devices utilizing them remains challenging due to their bulky nature and inevitable volume losses. Metasurfaces (MSs), a two-dimensional version of MMs, are able to overcome some of the problems mentioned above. MSs usually comprise periodic or nonperiodic subwavelength and ultrafine unit cells with metal or dielectric resonators [21]. MSs offer several key advantages over conventional technology used to create MMs. These include their cost-effectiveness,

less absorption compared to bulky MMs, and seamless integration due to their slender profile. Articles [22, 23] have demonstrated significant progress in achieving full control over electromagnetic waves through the use of MSs.

Numerous researchers are endeavoring to achieve the efficient control of electromagnetic wave propagation by using ultrathin structures. Compact devices with extensively integrated features are emerging as one of the most popular domains of modern technology. Given these benefits, they are highly promising candidates for effectively addressing the obstacles posed by the upcoming generation of transmitters and receivers. These future high-speed communication systems demand antennas, sensors, active components, filters, and other devices that are both highly accurate and efficient.

While numerous options exist, there is a strong need to enhance current polarizers or create novel polarization converters to meet the requirements of modern advanced technologies [24–27]. Wave polarization is incredibly rich in information, offering insights into material properties, surface topology, biological tissue properties, optical activity, and quantum properties. As a result, MSs with the ability to manipulate polarization can be applied in various fields such as remote sensing, biology, medicine, microscopy, optical communications, and quantum physics to create ultracompact and miniaturized optical systems. Typical chiral MSs convert the polarization of an incident wave in transmission or reflection modes. They can transform linear polarization to circular polarization and vice versa [28]. Additionally, they can also change the polarization from linear to linear with the rotation of the polarization plane [29]. This means that a transverse electrically polarized wave is converted into a transverse magnetically polarized wave, and vice versa.

MSs that are constructed according to the Huygens principle are notable for their exceptional effectiveness and simplicity in manipulating waves [30]. The Huygens principle operates on the premise that each point of a wavefront acts as a secondary source, either electric or magnetic, for the radiated waves. This principle establishes a qualitative correlation between the radiated field and its source when considering a dipole. The Huygens MS based on chiral inclusions offers more possibilities for manipulating the polarization of light through precise determination and adjustment of the induced electric and magnetic dipole moments of the chiral polarizable inclusions [31]. The chiral Huygens MS allows for independent control of the orthogonal polarizations of linearly polarized waves. This results in a highly efficient polarization conversion with unity transmittance or reflection coefficient, nonsplitting resonance, and broad transparency beyond the resonance band [32].

Several of the MSs mentioned above have limited capabilities and can only perform a single function. However, the increasing demands of modern society necessitate the development of technologies that can perform multiple functions simultaneously. The most straightforward approach to resolve this issue is through cascading. A number of works have successfully implemented this concept [33–36].

It is important to mention that the electromagnetic properties of MMs and MSs consisting of bulk smooth spiral elements have been intensively investigated over the last decades [37–41].

This research presents a multifunctional cascade MS designed to manipulate microwave electromagnetic waves. The structure consists of several thin MSs based on planar spirals with free space impedance. These MSs independently transform electromagnetic waves at different frequencies. The proposed MS includes three functional elements: a reflective cross-polarizer, a transmissive cross-polarizer, and a nonreflective absorber. A detailed analysis of electromagnetic dipole interactions is used to study the arrangement of chiral inclusions within the MS, which determines its polarization and absorption characteristics. The chiral inclusions are planar metal spirals aligned in the plane of the MSs (see Figure 1). These spirals are formed by metal traces on both sides of a printed circuit board (PCB) and are connected through vias in the dielectric substrate. The geometry and positioning of the spirals are carefully designed to match the input impedance of each MS to the impedance of free space. This condition is maintained over a wide frequency range, covering the operating frequencies of all MSs in the cascade. As a result, each MS operates independently without interfering with the others. The design is compatible with standard PCB fabrication technologies. The resulting cascade MS offers narrowband frequency selectivity, wide transparency outside of resonance, and structural simplicity. This paper presents experimental prototypes and their measured frequency responses. The proposed structures are promising for various applications, including antenna and array decoupling, frequency-selective wave control, and other microwave technologies.

2. Theoretical Calculations

Efficient polarization transformations can be realized using polarizable chiral inclusions. As demonstrated in previous studies [42], chirality directly influences the rotation of the polarization plane of transmitted or reflected waves. The maximum effect of a chiral inclusion on the wave occurs under the electromagnetic balance condition $|p| = |m|/c$ [42], where p and m denote the electric and magnetic dipole moments of the inclusion, respectively (the magnetic moment is defined as $m = IS_m$, with I being the loop current and S_m the area enclosed by the current loop).

We analyze a plane wave incident on a MS composed of subwavelength planar spirals arranged in a square lattice with a unit cell area S. The wave induces averaged electric $\widehat{\vec{p}}$ and magnetic $\widehat{\vec{m}}$ dipole moments per unit cell (the hat notation "$\widehat{\ \ }$" indicates unit cell moments, which may differ from those of individual spirals if the cell contains multiple elements). For an infinite MS, the reflected E_r and transmitted E_t fields can be expressed as follows [43, 44] (the cross symbol denotes the vector product):

$$\vec{E}_r = -\frac{j\omega\eta_0}{2S}\left(\widehat{\vec{p}} - \frac{1}{c}\vec{n}\times\widehat{\vec{m}}\right), \tag{1}$$

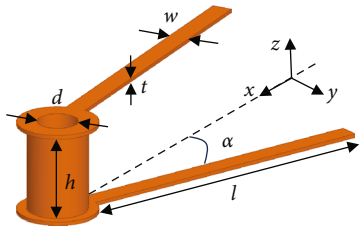

FIGURE 1: One-turn planar spiral (α is the half the angle between the metal strips; l is the length of the strip; d is the diameter of the hole with metalized walls; w is the width of the strip; t is the thickness of the strip; h is the height of the cylinder equal to the thickness of the board's dielectric substrate).

$$\vec{E}_t = \vec{E}_{\text{inc}} - \frac{j\omega\eta_0}{2S}\left(\widehat{\vec{p}} + \frac{1}{c}\vec{n}\times\widehat{\vec{m}}\right), \tag{2}$$

where ω is the cyclic frequency of the wave, $\eta_0 = \sqrt{\mu_0/\epsilon_0}$ is the free space wave impedance, $\vec{E}_{\text{inc}}$ is the electric field of the incident wave, c is the speed of light, $\vec{n} = -\vec{z}_0$ is the normal vector, and j is the imaginary unit.

The reflected and transmitted fields (1) and (2) arise when a linearly polarized plane wave propagating in the $-\vec{z}_0$ direction with the following polarization state is incident on the MS:

$$\vec{E}_{\text{inc}} = E_0\vec{x}_0, \vec{H}_{\text{inc}} = -\frac{E_0}{\eta_0}\vec{y}_0, \tag{3}$$

where $\vec{x}_0$, $\vec{y}_0$, and $\vec{z}_0$ are the coordinate system unit vectors and E_0 is the wave amplitude.

Components of vectors of electric and magnetic dipole moments read:

$$\widehat{\vec{p}} = \begin{bmatrix} \hat{p}\bullet\vec{x}_0 \\ \hat{p}\bullet\vec{y}_0 \\ \hat{p}\bullet\vec{z}_0 \end{bmatrix}, \widehat{\vec{m}} = \begin{bmatrix} \hat{m}\bullet\vec{x}_0 \\ \hat{m}\bullet\vec{y}_0 \\ \hat{m}\bullet\vec{z}_0 \end{bmatrix}. \tag{4}$$

Here, the point between the vectors denotes their scalar product. By substituting Conditions (3) and (4) into (1) and (2), we may derive the following expressions [44]:

$$E_r^x = -\frac{j\omega\eta_0}{2S}\left(\hat{p}_x - \frac{1}{c}\hat{m}_y\right), \tag{5}$$

$$E_t^x = E_0 - \frac{j\omega\eta_0}{2S}\left(\hat{p}_x + \frac{1}{c}\hat{m}_y\right), \tag{6}$$

$$E_r^y = -\frac{j\omega\eta_0}{2S}\left(\hat{p}_y + \frac{1}{c}\hat{m}_x\right), \tag{7}$$

$$E_t^y = -\frac{j\omega\eta_0}{2S}\left(\hat{p}_y - \frac{1}{c}\hat{m}_x\right). \tag{8}$$

Equations (5)–(8) demonstrate that the MS with chiral inclusions can become fully transparent at a specific wavelength only when its unit cells satisfy the electromagnetic balance condition $|\hat{p}_{x,y}| = |\hat{m}_{y,x}|/c$. A single planar spiral acting as a chiral inclusion primarily exhibits axial electric and magnetic dipole moments. For balanced moments, they must satisfy this condition. However, achieving the desired polarization transformations requires at least two spirals per unit cell. Perfect impedance matching (zero reflection) with air also needs this configuration. Together, these conditions ensure synchronous MS response. To balance a single spiral, we must first determine its individual dipole moments. While various methods exist for calculating dipole moments in arbitrarily shaped inclusions [34, 45], our study examines a simple one-turn metallic planar spiral. This structure serves as a fundamental chiral element that generates both electric and magnetic dipole moments at resonance frequency.

2.1. Theoretical Calculation of a Cross-Polarization Reflector. Consider a cross-polarization (i.e., rotating the plane of polarization by 90°) reflector with total reflection at the resonant frequency. In order to achieve a full cross-polarized reflectivity ($|R_{yx}|^2 = |E_r^y/E_0|^2 = 1$), the components of the reflected and transmitted fields must be equal. Part of this analysis extends the framework developed in our earlier work [44]:

$$E_r^x = 0, E_r^y = E_0 e^{j\phi_r^{cr}}, E_t^x = 0, E_t^y = 0. \tag{9}$$

Here, ϕ_r^{cr} is the initial phase of the reflected wave.

By substituting Condition (9) into (5)–(8), we can derive the final conditions for cross-polarized reflection. These conditions are based on the electric and magnetic dipole moments of the cell and can be expressed as follows:

$$\hat{p}_x = \frac{1}{c}\hat{m}_y = -j\frac{SE_0}{\omega\eta_0}, \tag{10}$$

$$\hat{p}_y = \frac{1}{c}\hat{m}_x = j\frac{SE_0}{\omega\eta_0}e^{j\phi_r^{cr}}. \tag{11}$$

These conditions imply that the unit cell must have equal orthogonal electric and magnetic dipole moments, with the phase of the reflected wave equal to $\phi_r^{cr} = \pi/2$.

Conditions (10) and (11) show the required orientation and components of the unit cell's electric and magnetic dipole moments. To meet these conditions, we use two right-handed spirals aligned along one axis in the cell and two left-handed spirals placed perpendicular to the first pair. This approach works for any MS with subwavelength polarized inclusions that need specific cross-polarized reflection coefficients.

We will choose the spiral's dimensions to create equal electric and magnetic responses (electromagnetic balance). This balance makes the MS rotate polarized waves by nearly 90° while having reflection at low level. The optimized spirals work efficiently across a wide frequency range around their resonance. This broad low-reflection bandwidth allows

combining multiple MSs with different functions, as long as they all operate within this frequency range.

2.2. Theoretical Calculation of a Transmissive Cross-Polarizer. Let us consider the equations describing the fields of a transmissive cross-polarizer that rotates the polarization plane of the transmitted wave by 90° at the resonant frequency. To achieve a full cross-polarized ability of the incident wave to transmit ($|T_{yx}|^2 = |E_t^y/E_0|^2 = 1$), the reflected and transmitted field components must be equal:

$$E_r^x = 0, E_t^x = 0, E_r^y = 0, E_t^y = E_0 e^{j\phi_t^{cr}}, \tag{12}$$

where ϕ_t^{cr} is the initial phase of the transmitted wave.

For a given polarization of the incident wave (3), the components of the reflected $E_{\mathrm{r}}^{\mathrm{x},y}$ and transmitted $E_{\mathrm{t}}^{\mathrm{x},y}$ fields can be determined using Equations (5)–(8). By substituting Condition (12) into Equations (5)–(8), one can obtain the final conditions for the transmission of a cross-polarized wave [44]:

$$\widehat{p}_x = \frac{1}{c}\widehat{m}_y = -j\frac{SE_0}{\omega\eta_0}, \tag{13}$$

$$\widehat{p}_y = -\frac{1}{c}\widehat{m}_x = j\frac{SE_0}{\omega\eta_0}e^{j\phi_t^{cr}}. \tag{14}$$

These conditions require that the x-component of the electric dipole moment matches the y-component of the magnetic moment (divided by the speed of light c), while other components must have opposite signs. This specific configuration enables complete 90° polarization rotation of transmitted waves without any energy loss. To satisfy these requirements, we can use either two identical chiral spirals (both left- or right-handed) arranged perpendicular to each other. Four identical spirals should be used to have uniaxial symmetrical MS properties that are oriented along both coordinate axes in the MS plane.

2.3. Theoretical Calculation of a Nonreflective Absorber. Consider the equations describing the reflected and transmitted fields in the context of an absorber of incident electromagnetic waves at the resonant frequency. In order to get complete absorption of the incident wave, the components of the reflected and transmitted fields ought to be equal:

$$E_r^x = 0, E_t^x = 0, E_r^y = 0, E_t^y = 0. \tag{15}$$

By substituting Condition (15) into Equations (5)–(8), we can obtain the final conditions for the absence of transmission and reflection of a wave with any polarization. These conditions are based on the electric and magnetic dipole moments of the cell and can be expressed as follows [44]:

$$\widehat{p}_x = \frac{1}{c}\widehat{m}_y = -j\frac{SE_0}{\omega\eta_0}, \tag{16}$$

$$\widehat{p}_y = \frac{1}{c}\widehat{m}_x = 0. \tag{17}$$

The resulting Conditions (16) and (17) reveal the necessary orientation and values of the components of the electric and magnetic dipole moments. This condition can be satisfied by using two orthogonal left-handed spirals and two orthogonal right-handed planar spirals with balanced moments.

3. Simulation and Experimental Results

3.1. Simulation Observations. In order to obtain the desired properties of the studied MSs, such as a reflective cross-polarizer, a transmissive cross-polarizer, and a nonreflective absorber, it is necessary to get the corresponding electromagnetic response of the unit cells. The balance between the electric dipole and magnetic moments of an individual element in the MS enables the attainment of the desired properties. A one-turn planar spiral (Figure 1) is regarded as an element of the MS. When subjected to an incident plane electromagnetic wave, dipole moments are induced in the one-turn planar spiral, which can be expressed through the components of the tensors of electric, magnetic, electromagnetic, and magnetoelectric polarizabilities.

The amplitudes of these polarizabilities, which are equal in absolute value, signify a balanced response from such a microresonator. To achieve a balanced electromagnetic response (i.e., the equality of the amplitudes of polarizabilities in resonance) from a helical microresonator, we conducted a numerical simulation of a one-turn planar spiral in vacuum, considering the frequency shift from the resonant frequency due to the presence of the Arlon AD255C dielectric. The procedure is thoroughly explained in [46, 47].

Based on the theoretical calculations mentioned above, we performed the simulation of the unit cells of the MSs consisting of left- and right-handed conducting planar spirals arranged on the Arlon AD255C dielectric substrate $\varepsilon_{\mathrm{r}} = 2.55$. Table 1 presents the geometric parameters of MSs with different functionalities.

Initially, the optimization of the linear dimensions of a single spiral is carried out. The optimization criterion is that the axial components of the polarizability tensors are approximately equal in absolute value at the resonance frequency. This indicates a balanced electromagnetic response to excitation by a linearly polarized plane wave. A detailed methodology was presented in our earlier works [43, 47]. Next, the unit cell is formed from the required number of spirals to implement a specific function. To obtain the maximum value of a particular coefficient at the resonance frequency, it is necessary to optimize the period (p) of the MS and the distance between the spirals in the unit cell (dx). Below are graphs of the frequency dependence of the cross-reflection coefficient for different parameter values.

Figure 2 illustrates that changing the distance between the spirals shifts the frequency of the maximum, while changing the period of the unit cell affects the peak level of the cross-reflection coefficient. In this way, the main parameters of the reflective cross-polarizer were optimized.

Figures 3a, 4a, and 5a demonstrate the unit cells of MSs constructed using one-turn planar spirals. Figures 3b, 4b, and 5b display the numerical simulation results.

TABLE 1: Geometric parameters of metasurfaces.

Metasurface	*l*, mm	*w*, mm	*α*, deg	*d*, mm	*h*, mm	*t*, *μ*m
Cross-polarization reflector	18.5	1.6	7.5	1.5	3.175	35
Transmissive cross-polarizer	15.8	1.6	8.5	1.5	3.175	35
Nonreflective absorber	13.8	1	10	1.5	3.175	35

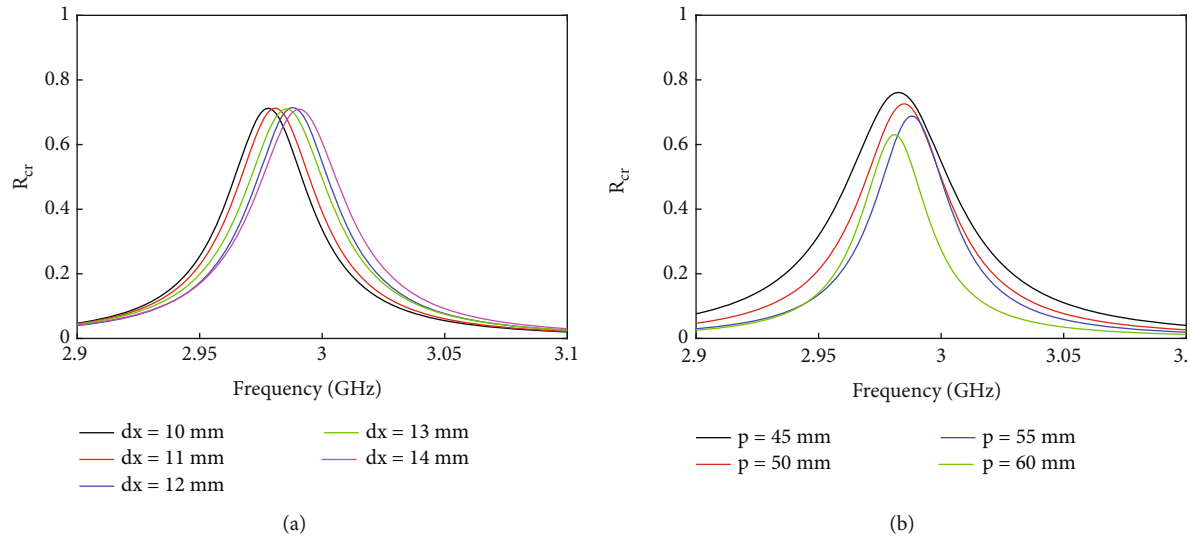

FIGURE 2: Frequency dependences of the cross-reflection coefficient with (a) the distance between the helices and (b) the period of the unit cell.

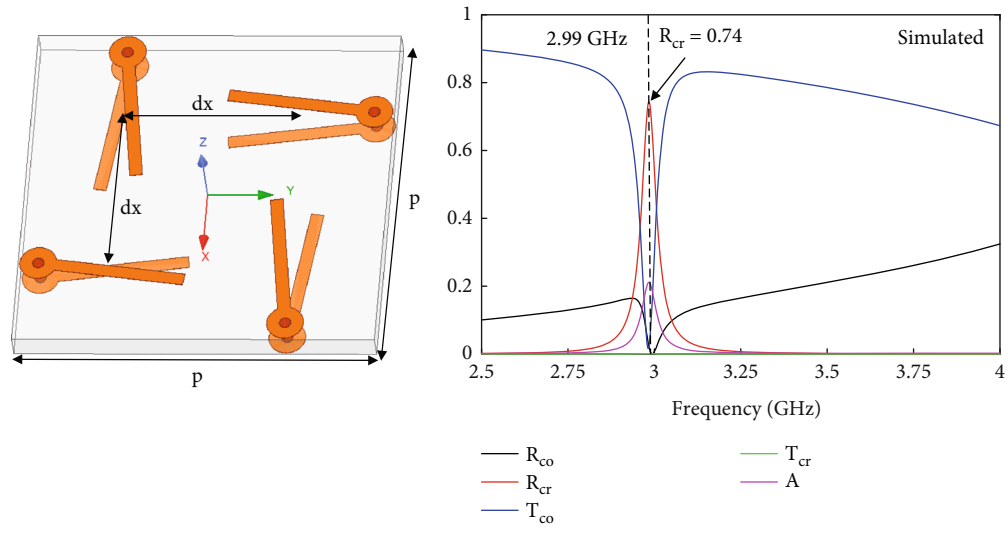

FIGURE 3: (a) Unit cell of a cross-polarization reflector based on one-turn planar spirals; (b) numerical simulation results of a cross-polarization reflector matched in wave impedance with free space.

The analysis of the plots in Figure 3b reveals that the coefficient of cross-polarized reflection (R_{cr}) approaches a value of 0.8 at the resonant frequency, while the coefficient of copolarized reflection (R_{co}) is nearly zero, indicating that the polarization plane of the reflected electromagnetic wave is rotated by 90°. The plots indicate that the transmission coefficient becomes zero at resonance. However, there is a 20.4% absorption of the electromagnetic wave, which can be attributed to losses in both the conductor (copper) and the Arlon AD255C dielectric.

The examination of the plots in Figure 4b demonstrates that the cross-polarized transmission coefficient (T_{cr}) approaches a value of 0.7 at the resonant frequency, while the coefficient of copolarized absorption (T_{co}) is virtually zero. These findings also suggest that the polarization plane of the transmitted electromagnetic wave is rotated by 90°.

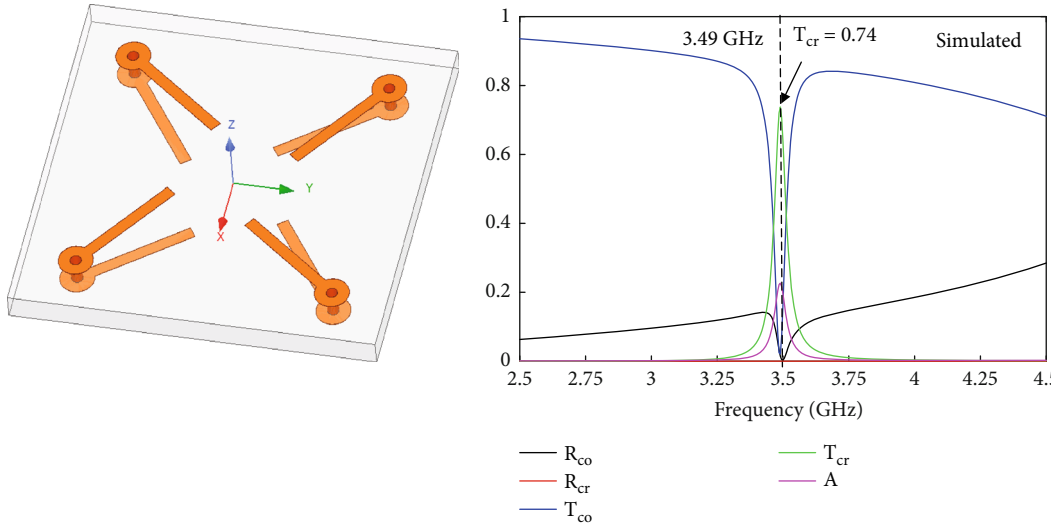

(a) (b)

FIGURE 4: (a) Unit cell of a transmissive cross-polarizer based on one-turn planar spirals; (b) numerical simulation results of a transmissive cross-polarizer matched in wave impedance with free space.

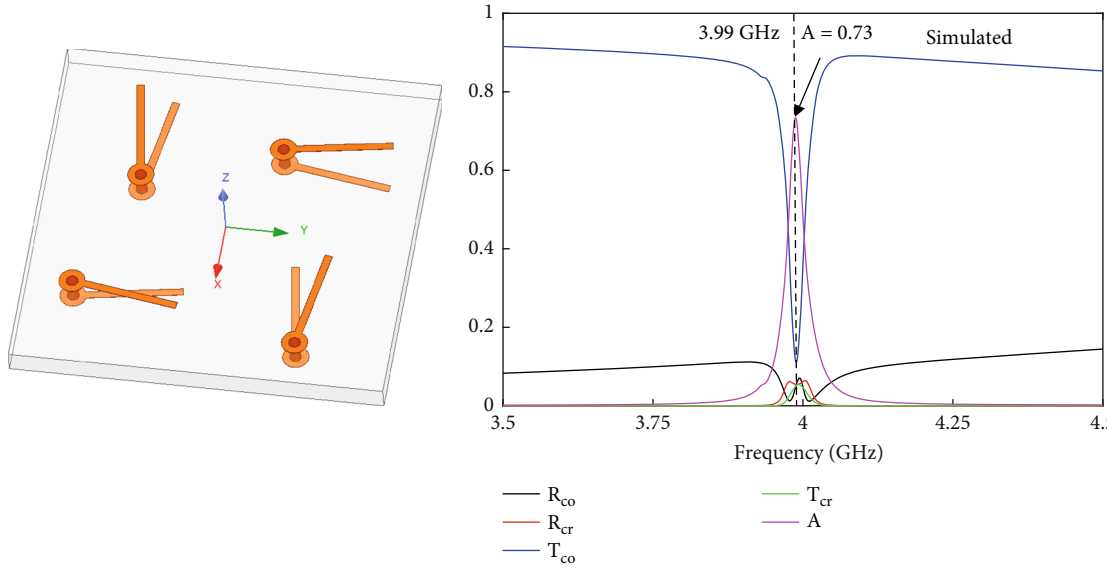

(a) (b)

FIGURE 5: (a) Unit cell of a nonreflective absorber based on one-turn planar spirals; (b) numerical simulation results of a nonreflective absorber on the Arlon AD255C substrate.

Through the optimization of the key parameters, it was determined that in order to achieve maximum absorption efficiency, it is necessary to position the spirals at right angles relative to each other. Additionally, it is important to have clearly defined identical coordinates for the location of the spirals with respect to the center of the unit cell with a side of 50 mm. The design features prevent achieving higher absorption values. The one-turn planar spiral has nonparallel electric and magnetic dipole moments, resulting in different values for the coefficients of copolarized and cross-polarized reflection, as well as similar transmission coefficients.

The analysis of the plots in Figure 4b reveals that the absorption coefficient (A) approaches a value of 0.7 at the resonant frequency of 4 GHz, while the copolarized reflection coefficient (R_{co}) and cross-polarized reflection coefficient (R_{cr}) do not surpass 6%.

Each MS has an ultrathin thickness in comparison to the resonant wavelength of approximately 0.037λ. This enables the integration of three different functions into a single multifunctional device by stacking layers in close proximity while maintaining an overall thickness that remains small compared to the wavelength. However, if the MSs are placed at a distance closer than 4 mm or 0.048λ, then the planar

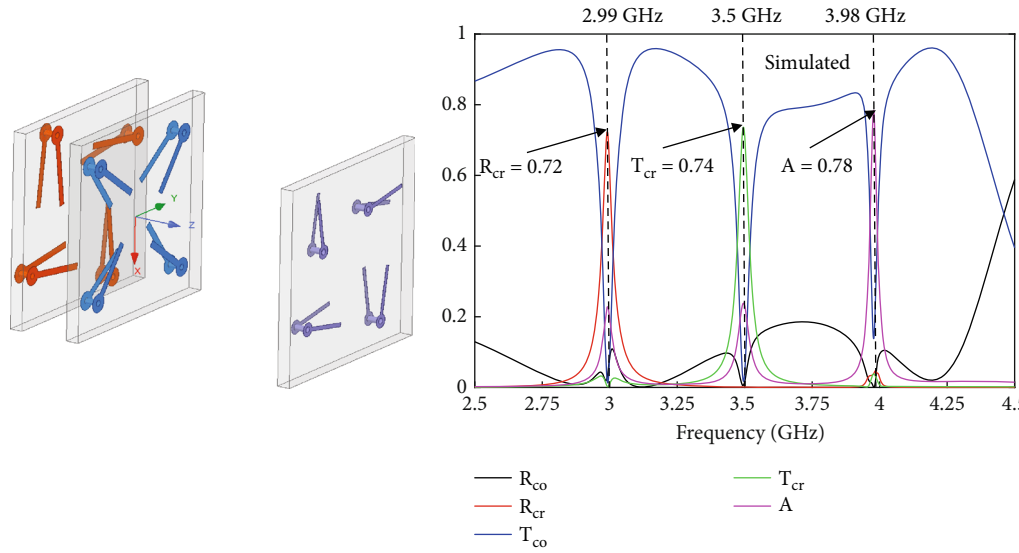

FIGURE 6: (a) Model of the metasurface cascade based on one-turn planar spirals; (b) numerical simulation results of the cascade of experimental samples with free space wave impedance.

spirals begin to interact with each other between layers. This disrupts the electromagnetic balance, causing the MS to lose its functional properties. The minimum gap required to prevent interlayer coupling is 6 mm (0.071λ).

In order to investigate the mutual influence and intercompatibility of the samples, the simulation of the MS cascade depicted in Figure 6a was conducted. The MSs were positioned at distances of 12 mm (0.143λ) and 33 mm (0.333λ), respectively.

The simulation results in Figure 6b show the independent nature of the properties exhibited by each layer. The distances between MSs were deliberately made different to demonstrate that the layer separation does not affect their individual functional performance. The MS exhibits cross-polarization reflector properties at a frequency of 3 GHz. At 3.5 GHz, it revealed MS properties enabling cross-polarization transmission. Finally, at 4 GHz, the MS demonstrated properties with a nonreflective absorber function.

Figure 7 shows the numerical study to examine the influence of a multifunctional cascade of MSs on the characteristics of the wave at an oblique incidence.

The studies showed that the proposed structure has quite stable characteristics up to 30°. Cross-polarization reflection and absorption are not lower than 0.6 in a wide range of incidence angles up to 50°.

3.2. Experiment. The final stage of our research was to fabricate prototypes using PCB technology according to the design parameters and conduct experimental measurements. The experimental measurements were carried out in an anechoic chamber in the Electromagnetic Metamaterials Research Laboratory of Nanjing University of Science and Technology. Two horn antennas and a vector network analyzer were used to measure the reflection (Figure 8a) and transmission Figure 8b modes.

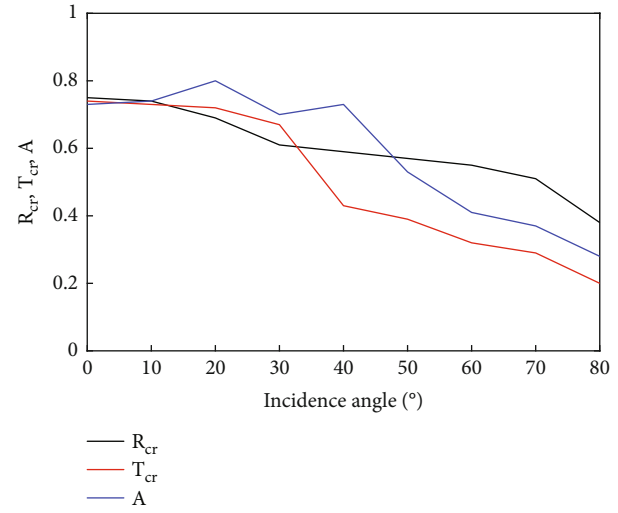

FIGURE 7: Effect of the incidence angle on the reflection, transmission, and absorption coefficients of a cascade of metasurfaces.

All fabricated samples have dimensions of 410 × 410 mm. The obtained MS (Figure 9a) implements cross-polarization reflection of incident waves. The experimental results (Figure 9b) show a good degree of agreement with numerical simulation. The coefficient R_{cr} at the resonance frequency of 3 GHz was about 75%. It should be noted that the coefficient R_{co} is high, which differs from the numerical simulation results (Figure 3b). This may be caused by the sample imperfection after the fabrication process.

The MS implementing the cross-polarization transmission function of incident waves is shown in Figure 10a. The experimental value of the resonant frequency and transmittance for the transmitting cross-polarizer has good agreement with the simulation results (Figures 4b and 10b). Also,

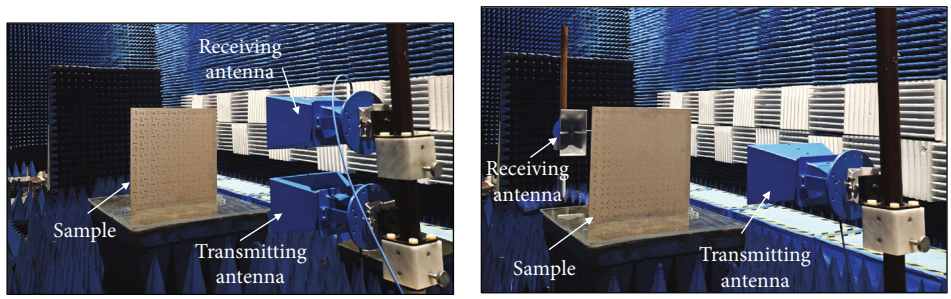

(a) (b)

FIGURE 8: Laboratory setup for conducting experimental studies on (a) reflection and (b) transmission.

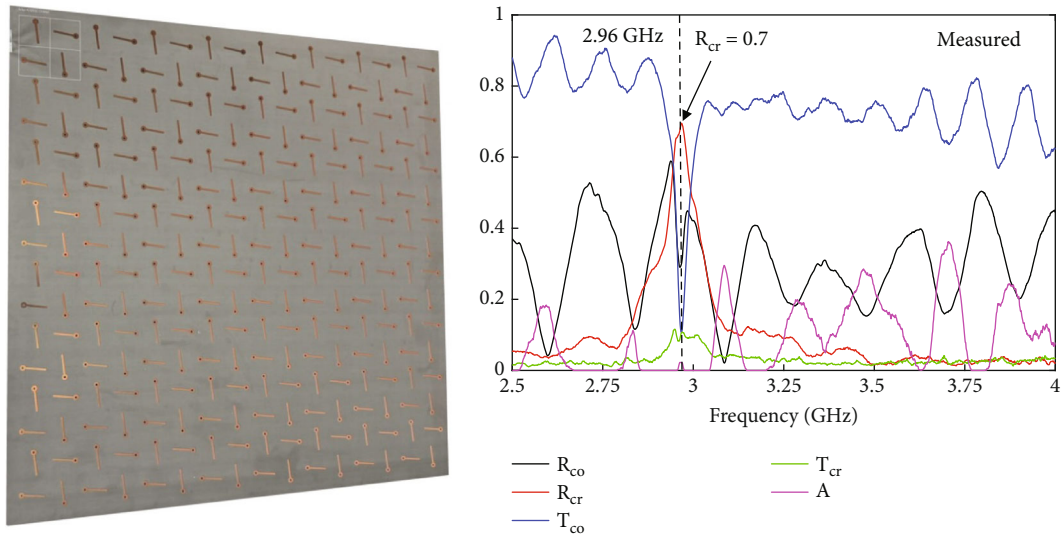

(a) (b)

FIGURE 9: (a) Experimental sample of a cross-polarization reflector using one-turn planar spirals on the Arlon AD255C substrate; (b) experimental results.

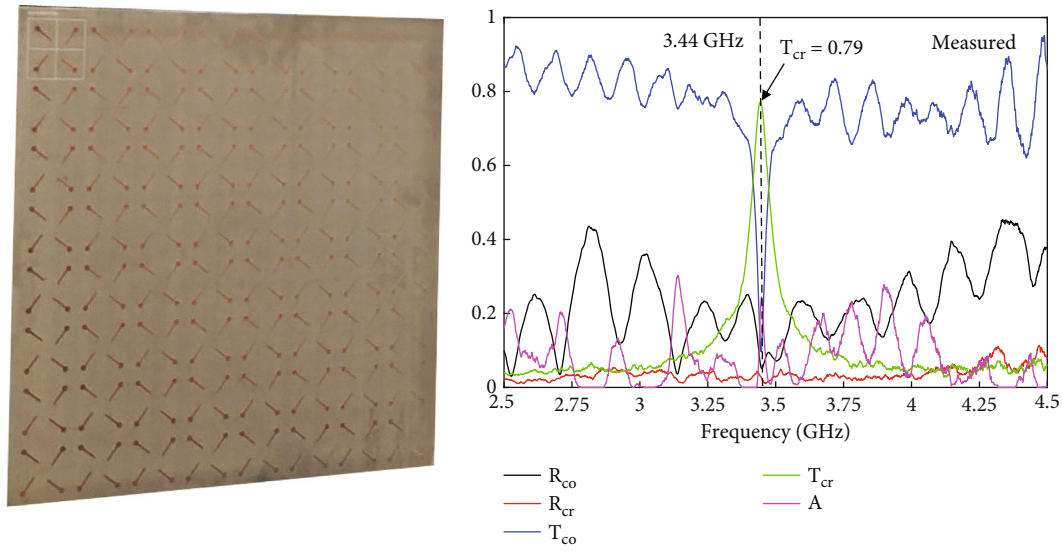

(a) (b)

FIGURE 10: (a) Experimental sample of a transmissive cross-polarizer using one-turn planar spirals on the Arlon AD255C substrate; (b) experimental results.

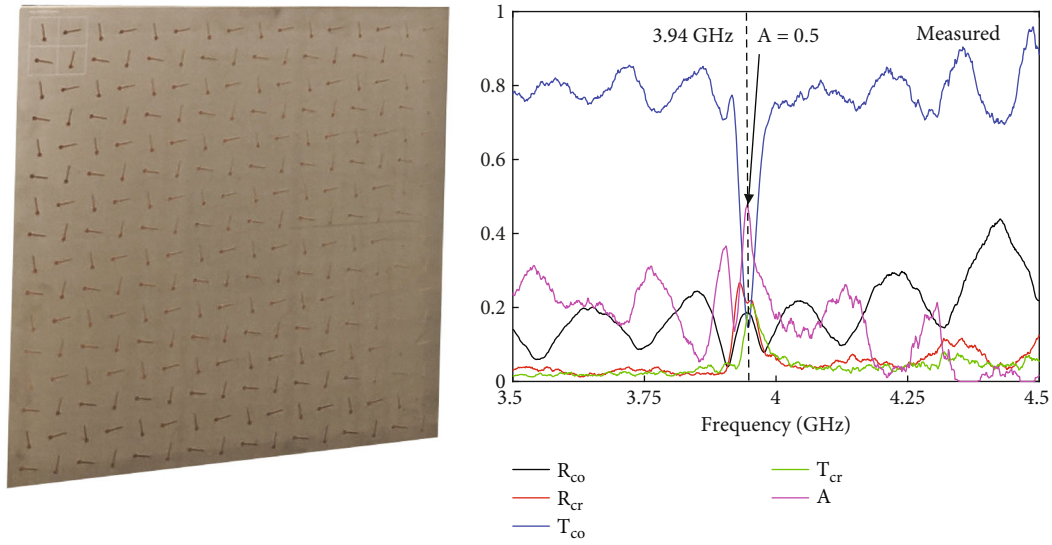

(a) (b)

FIGURE 11: (a) Experimental sample of a nonreflective absorber using one-turn planar spirals on the Arlon AD255C substrate; (b) experimental results.

the MS is transparent outside the resonant frequency in the entire frequency band.

The photo of experimental sample and measured results of the nonreflecting absorber are shown in Figure 11a,b, respectively. The resonance frequency is slightly shifted toward low frequencies and is 3.94 GHz. The absorption maximum is lower than the numerically calculated values and does not exceed 0.56. The values of the R_{cr} and T_{cr} coefficients at the resonance frequency indicate an imbalance of single-turn planar spirals in the unit cell. This mismatching can be explained by the inaccurate correspondence of the permittivity and loss tangent of the real Arlon AD255C dielectric and the one specified during simulation, as well as by an inaccuracy in the sample's manufacturing process.

Figure 12a,b shows a MS cascade with measured reflection and transmission coefficients, which is capable of simultaneously performing several functional tasks. The distances between the MSs were taken to be 12 and 33 mm, respectively. Different values were taken to show the independence of the MSs from the distance and the absence of mutual influence on each other due to different proximity.

The findings from the experimental studies demonstrated a strong correlation with numerical simulations, highlighting the potential of this MS cascade to function as an independent and mutually compatible converter for waves across different frequencies.

All experimental graphs show a shift in the resonance frequency toward lower frequencies compared to the simulation results, by approximately 0.05 GHz. This shift is attributed to the discrepancy in the dielectric permittivity used in the simulation ($\varepsilon_r = 2.55$) and that of the actual samples (in practice, ε_r was higher).

It can also be stated that the absorber is more sensitive to changes in linear dimensions. Inaccuracies in the fabrication of flat spirals cause electromagnetic imbalance in the structure and reduce the absorption coefficient.

The mismatch between experimental results and simulation may also stem from slight wave reflections between layers. These reflections could have affected the functionality of each layer.

The proposed multifunctional cascade of MSs demonstrates a distinctive design with several notable advantages. Below, we highlight the key features that distinguish the novelty of our work from many existing studies:

- Each individual layer is ultrathin, with a thickness of only 0.037λ. The vast majority of work is performed according to this parameter [48].
- The operation of each individual function is inherently designed to be frequency-selective.
- The proposed structure remains transparent over a broad frequency range outside the resonance, with its performance limited solely by the properties of the dielectric substrate. In this regard, our design outperforms the majority of existing solutions.
- The multifunctional cascade of MSs is a passive device. In contrast, many existing multifunctional designs rely on active (switching) elements, such as PIN diodes [49], which increase system complexity due to the required control circuitry, additional losses, and other associated challenges.

It is important to emphasize that the three demonstrated functions do not represent the full potential of functionalities that can be realized using planar spiral-based structures.

From a practical standpoint, employing standard PCB fabrication technologies makes the proposed solution economically viable and readily scalable across various frequency bands.

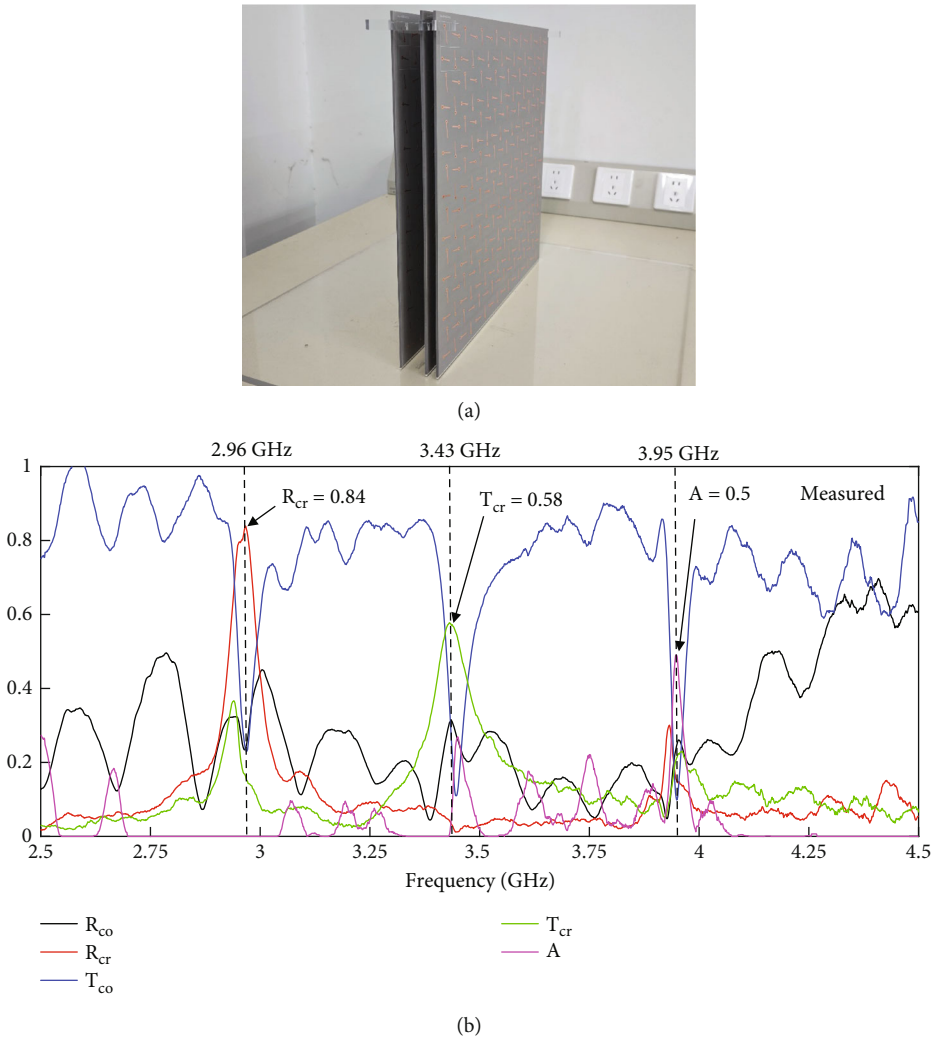

FIGURE 12: (a) Cascade of experimental samples based on one-turn planar spirals; (b) experimental results.

The developed MS cascade, which performs cross-polarization reflection and transmission functions, is of considerable interest for modern microwave technologies. It enables efficient control of the polarization of both reflected and transmitted waves. The device can be used in radar systems to create polarization filters that enhance target discrimination and interference suppression by transforming the polarization of the reflected or transmitted signal. This solution is also suitable for communication antenna systems, where it enables polarization multiplexing. In radar applications, it supports interference-resistant filtering and improved target selection. Additionally, it can be integrated into measurement setups for calibrating the polarization characteristics of microwave components. Thanks to its planar design and compatibility with PCB technologies, the polarizers can be easily integrated into existing microwave systems. This is especially valuable for compact and energy-efficient devices.

The third function, absorption, is also highly useful in antenna and radar systems. It helps reduce mutual coupling in antenna arrays, suppress unwanted signals, and control the radiation pattern in a frequency-selective manner. These features are especially relevant for modern radio systems operating in complex electromagnetic environments, where minimizing mutual interference is critical. The unique ability to selectively absorb radiation at a specific frequency, while remaining transparent at others, opens new opportunities for object concealment and protection of critical electronics. Unlike conventional screens that reflect or absorb the entire spectrum, our design provides a targeted response without disrupting the operation of nearby radio devices.

4. Conclusion

Theoretically proved and empirically validated, it is possible to create MSs with wave impedance of free space on the basis of one-turn planar spirals with functions of a reflective cross-polarizer, a transmissive cross-polarizer, and a nonreflective absorber. The feasibility of employing a cascade of MSs to perform multiple functional tasks simultaneously has been illustrated. Each designed MS possesses a free space impedance over a sufficiently wide frequency range that encompasses the operating frequencies of all MSs. This

characteristic allows for the autonomous and mutually non-interfering functioning of all MSs in the cascade.

Data Availability Statement

The data that support the findings of this study are available from the corresponding author upon reasonable request.

Conflicts of Interest

The authors declare no conflicts of interest.

Funding

The study is funded by the Belarusian Republican Foundation for Fundamental Research (10.13039/100007595) (F23KI-027, F22KITG-021).

References

[1] D. R. Smith, W. J. Padilla, D. C. Vier, S. C. Nemat-Nasser, and S. Schultz, "Composite Medium With Simultaneously Negative Permeability and Permittivity," *Physical Review Letters* 84, no. 18 (2000): 4184–4187.

[2] D. Schurig, J. J. Mock, B. J. Justice, et al., "Metamaterial Electromagnetic Cloak at Microwave Frequencies," *Science* 314, no. 5801 (2006): 977–980.

[3] D. Schurig and D. R. Smith, "Negative-Index Lens Aberrations," *Physical Review E* 70, no. 6 (2004): 264–277, https://doi.org/10.1103/PhysRevE.70.065601.

[4] Y. Shen, Z. Pei, Y. Pang, J. Wang, A. Zhang, and S. Qu, "An Extremely Wideband and Lightweight Metamaterial Absorber," *Journal of Applied Physics* 117, no. 22 (2015): 224503.

[5] N. I. Landy, S. Sajuyigbe, J. J. Mock, D. R. Smith, and W. J. Padilla, "Perfect Metamaterial Absorber," *Physical Review Letters* 100, no. 20 (2008): 207402.

[6] X. Ni, N. K. Emani, A. V. Kildishev, A. Boltasseva, and V. M. Shalaev, "Broadband Light Bending With Plasmonic Nanoantennas," *Science* 335, no. 6067 (2012): 427, https://doi.org/10.1126/science.1214686.

[7] Y. Li, J. Zhang, S. Qu, et al., "Wideband Radar Cross Section Reduction Using Two-Dimensional Phase Gradient Metasurfaces," *Applied Physics Letters* 104, no. 22 (2014): 221110, https://doi.org/10.1063/1.4881935.

[8] X. Li, S. Xiao, B. Cai, Q. He, T. J. Cui, and L. Zhou, "Flat Metasurfaces to Focus Electromagnetic Waves in Reflection Geometry," *Optics Letters* 37, no. 23 (2012): 4940–4942, https://doi.org/10.1364/OL.37.004940.

[9] K. Wang, J. Zhao, Q. Cheng, D. S. Dong, and T. J. Cui, "Broadband and Broad-Angle Low-Scattering Metasurface Based on Hybrid Optimization Algorithm," *Scientific Reports* 4, no. 1 (2014): 5935, https://doi.org/10.1038/srep05935.

[10] F. Costa, A. Monorchio, and G. Manara, "Wideband Scattering Diffusion by Using Diffraction of Periodic Surfaces and Optimized Unit Cell Geometries," *Scientific Reports* 6, no. 1 (2016): 25458, https://doi.org/10.1038/srep25458.

[11] N. Yu, P. Genevet, M. A. Kats, et al., "Light Propagation With Phase Discontinuities: Generalized Laws of Reflection and Refraction," *Science* 334, no. 6054 (2011): 333–337, https://doi.org/10.1126/science.1210713.

[12] X. Ma, M. Pu, X. Li, et al., "A Planar Chiral Meta-Surface for Optical Vortex Generation and Focusing," *Scientific Reports* 5, no. 1 (2015): 10365, https://doi.org/10.1038/srep10365.

[13] Y. Yang, W. Wang, P. Moitra, I. I. Kravchenko, D. P. Briggs, and J. Valentine, "Dielectric Meta-Reflectarray for Broadband Linear Polarization Conversion and Optical Vortex Generation," *Nano Letters* 14, no. 3 (2014): 1394–1399, https://doi.org/10.1021/nl4044482.

[14] A. Arbabi, Y. Horie, M. Bagheri, and A. Faraon, "Dielectric Metasurfaces for Complete Control of Phase and Polarization With Subwavelength Spatial Resolution and High Transmission," *Nature Nanotechnology* 10, no. 11 (2015): 937–943, https://doi.org/10.1038/nnano.2015.186.

[15] G. Zheng, H. Mühlenbernd, M. Kenney, G. Li, T. Zentgraf, and S. Zhang, "Metasurface Holograms Reaching 80% Efficiency," *Nature Nanotechnology* 10, no. 4 (2015): 308–312, https://doi.org/10.1038/nnano.2015.2.

[16] M. Born, E. Wolf, A. B. Bhatia, et al., *Principles of Optics* (Cambridge University Press, 2013), https://doi.org/10.1017/CBO9781139644181.

[17] O. Quevedo-Teruel, H. Chen, A. Díaz-Rubio, et al., "Roadmap on Metasurfaces," *Journal of Optics* 21, no. 7 (2019): 073002, https://doi.org/10.1088/2040-8986/ab161d.

[18] A. Alexopoulos, "Effective-Medium Theory of Surfaces and Metasurfaces Containing Two-Dimensional Binary Inclusions," *Physical Review E* 81, no. 4 (2010): 046607, https://doi.org/10.1103/PhysRevE.81.046607.

[19] X. Zhang and Y. Wu, "Effective Medium Theory for Anisotropic Metamaterials," *Scientific Reports* 5, no. 1 (2015): 7892, https://doi.org/10.1038/srep07892.

[20] J. Mei, Y. Wu, and Z. Liu, "Effective Medium of Periodic Fluid-Solid Composites," *Europhysics Letters* 98, no. 5 (2012): 54001, https://doi.org/10.1209/0295-5075/98/54001.

[21] C. L. Holloway, E. F. Kuester, J. A. Gordon, J. O'Hara, J. Booth, and D. R. Smith, "An Overview of the Theory and Applications of Metasurfaces: The Two-Dimensional Equivalents of Metamaterials," *IEEE Antennas and Propagation Magazine* 54, no. 2 (2012): 10–35, https://doi.org/10.1109/MAP.2012.6230714.

[22] L. Zhang, S. Mei, K. Huang, and C. W. Qiu, "Advances in Full Control of Electromagnetic Waves With Metasurfaces," *Advanced Optical Materials* 4, no. 6 (2016): 818–833, https://doi.org/10.1002/adom.201500690.

[23] S. B. Glybovski, S. A. Tretyakov, P. A. Belov, Y. S. Kivshar, and C. R. Simovski, "Metasurfaces: From Microwaves to Visible," *Physics Reports* 634 (2016): 1–72, https://doi.org/10.1016/j.physrep.2016.04.004.

[24] S. Iqbal, S. Liu, J. Luo, L. Zhang, H. A. Madni, and T. J. Cui, "Controls of Transmitted Electromagnetic Waves for Diverse Functionalities Using Polarization-Selective Dual-Band 2 Bit Coding Metasurface," *Journal of Optics* 22, no. 1 (2020): 015104, https://doi.org/10.1088/2040-8986/ab5e18.

[25] Y. Hu, X. Wang, X. Luo, et al., "All-Dielectric Metasurfaces for Polarization Manipulation: Principles and Emerging Applications," *Nanophotonics* 9, no. 12 (2020): 3755–3780, https://doi.org/10.1515/nanoph-2020-0220.

[26] Y. Huang, T. Xiao, Z. Xie, et al., "Single-Layered Reflective Metasurface Achieving Simultaneous Spin-Selective Perfect Absorption and Efficient Wavefront Manipulation," *Advanced Optical Materials* 9, no. 5 (2021): 2001663, https://doi.org/10.1002/adom.202001663.

[27] S. Yu, J. Cheng, Z. Li, et al., "Electromagnetic Wave Manipulation Based on Few-Layer Metasurfaces and Polyatomic Metasurfaces," *ChemPhysMater* 1, no. 1 (2022): 6–16, https://doi.org/10.1016/j.chphma.2021.09.001.

[28] S. Yan and G. A. Vandenbosch, "Compact Circular Polarizer Based on Chiral Twisted Double Split-Ring Resonator," *Applied Physics Letters* 102, no. 10 (2013): https://doi.org/10.1063/1.4794940.

[29] M. Mutlu and E. Ozbay, "A Transparent 90 Polarization Rotator by Combining Chirality and Electromagnetic Wave Tunneling," *Applied Physics Letters* 100, no. 5 (2012): https://doi.org/10.1063/1.3682591.

[30] M. Chen, M. Kim, A. M. Wong, and G. V. Eleftheriades, "Huygens' Metasurfaces From Microwaves to Optics: A Review," *Nanophotonics* 7, no. 6 (2018): 1207–1231, https://doi.org/10.1515/nanoph-2017-0117.

[31] C. Rockstuhl, T. Zentgraf, H. Guo, et al., "Resonances of Split-Ring Resonator Metamaterials in the Near Infrared," *Applied Physics B* 84, no. 1-2 (2006): 219–227, https://doi.org/10.1007/s00340-006-2205-2.

[32] Z. Sun, B. Sima, J. Zhao, and Y. Feng, "Electromagnetic Polarization Conversion Based on Huygens' Metasurfaces With Coupled Electric and Magnetic Resonances," *Optics Express* 27, no. 8 (2019): 11006–11017, https://doi.org/10.1364/OE.27.011006.

[33] X. Cai, R. Tang, H. Zhou, et al., "Dynamically Controlling Terahertz Wavefronts With Cascaded Metasurfaces," *Advanced Photonics* 3, no. 3 (2021): 036003, https://doi.org/10.1117/1.AP.3.3.036003.

[34] A. A. Elsakka, V. S. Asadchy, I. A. Faniayeu, S. N. Tcvetkova, and S. A. Tretyakov, "Multifunctional Cascaded Metamaterials: Integrated Transmitarrays," *IEEE Transactions on Antennas and Propagation* 64, no. 10 (2016): 4266–4276, https://doi.org/10.1109/TAP.2016.2594824.

[35] Q. Li, X. Li, Y. Chen, et al., "High-Performance Dual-Band Frequency-Selective Rasorber Based on Cascaded Metasurface," *Frontiers in Materials* 9 (2022): 949076, https://doi.org/10.3389/fmats.2022.949076.

[36] P. Yang, R. Yang, and Y. Li, "Compact Cascaded Meta-Surface System for Controlling the Spin and Orbital Angular Momentum of Electromagnetic Fields Simultaneously," *Optics Express* 29, no. 13 (2021): 20229–20239, https://doi.org/10.1364/OE.428494.

[37] I. V. Semchenko, S. A. Khakhomov, S. A. Tretyakov, and A. H. Sihvola, "Electromagnetic Waves in Artificial Chiral Structures With Dielectric and Magnetic Properties," *Electromagnetics* 21, no. 5 (2001): 401–414, https://doi.org/10.1080/027263401300364973.

[38] I. V. Semchenko and S. A. Khakhomov, "Artificial Uniaxial Bianisotropic Media at Oblique Incidence of Electromagnetic Waves," *Electromagnetics* 22, no. 1 (2002): 71–84, https://doi.org/10.1080/027263402753427673.

[39] I. V. Semchenko, S. A. Khakhomov, and A. L. Samofalov, "Polarization Plane Rotation of Electromagnetic Waves by the Artificial Periodic Structure With One-Turn Helical Elements," *Electromagnetics* 26, no. 3-4 (2006): 219–233, https://doi.org/10.1080/02726340600570302.

[40] I. V. Semchenko, S. A. Khakhomov, and A. L. Samofalov, "Helices of Optimal Shape for Nonreflecting Covering," *European Physical Journal Applied Physics* 49, no. 3 (2010): 33002, https://doi.org/10.1051/epjap/2009149.

[41] I. V. Semchenko, S. A. Khakhomov, V. S. Asadchy, et al., "Investigation of Electromagnetic Properties of a High Absorptive, Weakly Reflective Metamaterial-Substrate System With Compensated Chirality," *Journal of Applied Physics* 121, no. 1 (2017): https://doi.org/10.1063/1.4973679.

[42] I. V. Semchenko, S. A. Khakhomov, and A. L. Samofalov, "Transformation of the Polarization of Electromagnetic Waves by Helical Radiators," *Journal of Communications Technology and Electronics* 52, no. 8 (2007): 850–855, https://doi.org/10.1134/S1064226907080037.

[43] F. S. Cuesta, I. A. Faniayeu, V. S. Asadchy, and S. A. Tretyakov, "Planar Broadband Huygens' Metasurfaces for Wave Manipulations," *IEEE Transactions on Antennas and Propagation* 66, no. 12 (2018): 7117–7127, https://doi.org/10.1109/TAP.2018.2869256.

[44] I. A. Faniayeu, V. S. Asadchy, and I. A. Fanyaev, "Polarization Control With Helical Metasurfaces," *Crystals* 10, no. 9 (2020): 726, https://doi.org/10.3390/cryst10090726.

[45] Y. Ra'di, V. S. Asadchy, and S. A. Tretyakov, "One-Way Transparent Sheets," *Physical Review B* 89, no. 7 (2014): 075109, https://doi.org/10.1103/PhysRevB.89.075109.

[46] A. Ishimaru, S.-W. Lee, Y. Kuga, and V. Jandhyala, "Generalized Constitutive Relations for Metamaterials Based on the Quasi-Static Lorentz Theory," *IEEE Transactions on Antennas and Propagation* 51, no. 10 (2003): 2550–2557, https://doi.org/10.1109/TAP.2003.817565.

[47] V. S. Asadchy, I. A. Faniayeu, Y. Ra'di, and S. A. Tretyakov, "Determining Polarizability Tensors for an Arbitrary Small Electromagnetic Scatterer," *Photonics and Nanostructures-Fundamentals and Applications* 12, no. 4 (2014): 298–304, https://doi.org/10.1016/j.photonics.2014.04.004.

[48] R. Dutta, J. Ghosh, Z. Yang, and X. Zhang, "Multi-Band Multi-Functional Metasurface-Based Reflective Polarization Converter for Linear and Circular Polarizations," *IEEE Access* 9 (2021): 152738–152748, https://doi.org/10.1109/ACCESS.2021.3128190.

[49] P. Wang, Y. Zhang, Y. Wang, H.-C. Zhou, and Z.-M. Yan, "Multifunctional Polarization Converter Based on Multilayer Reconfigurable Metasurface," *Defence Technology* 28 (2023): 136–145, https://doi.org/10.1016/j.dt.2022.12.008.